

Quark Density in Lattice QC₂D at Imaginary and Real Chemical Potential

A. M. Begun and N. V. Gerasimeniuk

Pacific Quantum Center, Far Eastern Federal University, 690950 Vladivostok, Russia

V. G. Bornyakov

*Institute for High Energy Physics of the NRC Kurchatov Institute, 142281 Protvino, Russia,
Institute of Theoretical and Experimental Physics of the NRC Kurchatov Institute, 117218 Moscow, Russia
Pacific Quantum Center, Far Eastern Federal University, 690950 Vladivostok, Russia*

V. A. Goy

*Institut Denis Poisson CNRS/UMR 7013, Université de Tours, 37200 France
Pacific Quantum Center, Far Eastern Federal University, 690950 Vladivostok, Russia*

A. Nakamura

*RCNP, Osaka University, Osaka 567-0047, Japan
Pacific Quantum Center, Far Eastern Federal University, 690950 Vladivostok, Russia*

R. N. Rogalyov

Institute for High Energy Physics of the NRC “Kurchatov Institute”, 142281 Protvino, Russia

V. Vovchenko

Nuclear Science Division, Lawrence Berkeley National Laboratory, 1 Cyclotron Road, Berkeley, CA 94720, USA

We study lattice two-color QCD (QC₂D) with two flavors of staggered fermions at imaginary and real quark chemical potential μ_q and $T > T_c$. We employ various methods of analytic continuation of the quark number density from imaginary to real quark chemical potentials μ_q , including series expansions as well as based on phenomenological models, and study their accuracy by comparing the results to the lattice data. Below the Roberge-Weiss temperature, $T < T_{RW}$, we find that the cluster expansion model provides an accurate analytic continuation of the baryon number density in the studied range of chemical potentials. On the other hand, the behavior of the reconstructed canonical partition functions indicate that the available models may require corrections at high quark densities. At $T > T_{RW}$ we show that the analytic continuation to the real values of μ_q based on trigonometric functions works equally well with the conventional method based on the Taylor expansion in powers of μ_q .

I. INTRODUCTION

Studies of strongly interacting matter under extreme conditions are among the most important topics in modern high-energy physics. Experimentally, the QCD phase structure is probed by heavy-ion collisions (HIC) at LHC [1], RHIC [2], and SPS [3], where a dense and hot fireball of QCD matter is created and then expands and evolves from the state of strongly-coupled quark-gluon plasma (sQGP) to the hadron resonance gas. In the plane “baryon chemical potential – temperature” ($\mu_B - T$) these two phases are separated by a transition region. This region corresponds to an analytic crossover at vanishing baryon density, as established from first-principle lattice QCD simulations [4]. It is feasible that the transition line turns into a first-order phase transition at large baryon densities with an associated QCD critical end point (CEP). Analysis of the QCD phase structure at finite baryon densities is in the focal point of the beam energy scans at RHIC [5, 6] and SPS [7], which will be supplemented by the future HIC experiments at FAIR (GSI) [8] and at NICA (JINR) [9]. It is hoped that these experiments will be able to answer the question of the existence of the CEP.

Presently we have no proper theoretical understanding of the phase diagram of QCD in the $\mu_B - T$ plane from first principles. In particular, even the dependence of the baryon-number density n_B on the quark chemical potential $\mu_q \equiv \mu_B/N_c$ remains an open question, though we know that n_B increases with increasing μ_q and $n_B(\mu_q = 0) = 0$. While at $\mu_q = 0$ the QCD phase diagram has been successfully studied theoretically in the framework of lattice QCD, at finite μ_q values relevant for the CEP search this approach is plagued by the sign problem.

Even though direct lattice simulations at $\mu_q \neq 0$ are currently not possible, the thermodynamical quantities can be calculated at small $\theta \equiv \mu_q/T$ indirectly. Two approaches have commonly been employed: the first one is based on Taylor expansion in θ around $\theta = 0$ [10–13] while the second one employs analytical continuation

from imaginary θ , where sign problem is absent, to real θ [14–22].

In this work we study two-color QCD (QC₂D) on the lattice, which have received considerable attention in the literature, see, e.g. [23–46] and references therein. The keen interest in QC₂D and QCD-like theories stems from two reasons: first, they are expected to share common properties with full QCD in some parts of their phase diagrams, and, second, they are numerically tractable, thus allowing to test methods that can later be used in QCD. In particular, the lattice simulations of QC₂D can be performed both at imaginary and real μ_q . We use this fact to analyze the efficiency of various procedures based on the analytic-continuation method and select the optimal one. The results of earlier studies along these lines were presented in Refs. [28, 30–32].

The paper is organized as follows. In Sec. II we describe details of our lattice simulations. Secs. III and IV explore the performance of various analytic continuation procedures at low and high temperatures, respectively. Summary in Sec. V closes the article.

II. DEFINITIONS AND DETAILS OF SIMULATION

The grand canonical partition function $Z_{GC} \left(\frac{\mu_q}{T} \equiv \theta, T, V \right)$ can be written as a sum of the canonical ones $Z_C(n, T, V)$:

$$Z_{GC}(\theta, T, V) = \sum_{n=-\infty}^{\infty} Z_C(n, T, V) \xi^n, \quad (1)$$

where $\xi = e^\theta$ is the fugacity. We refer to the expression given by Eq. (1) as the fugacity expansion. Here and below, the variable $\theta = \frac{\mu_q}{T} = \theta_R + i\theta_I$ is employed. The inverse of the fugacity expansion has the form [47]

$$Z_C(n, T, V) = \int_0^{2\pi} \frac{d\theta_I}{2\pi} e^{-in\theta_I} Z_{GC}(\theta_I, T, V), \quad (2)$$

where $Z_{GC}(\theta_I, T, V)$ is the grand canonical partition function at imaginary chemical potential ($\theta_R = 0$). Z_{GC} is a periodic function of θ_I : $Z_{GC}(\theta_I, T, V) = Z_{GC}(\theta_I + 2\pi/N_c, T, V)$. As a consequence of this periodicity the canonical partition functions $Z_C(n, T, V)$ are nonzero only for $n = N_c \cdot k$ for $k \in \mathbb{Z}$. This symmetry is called the Roberge-Weiss symmetry [48].

Below we will mostly use the following dimensionless variable representing the baryon number in the lattice volume $V = a^3 N_s^3$ under consideration

$$B = \frac{n_q V}{N_c} \quad (3)$$

instead of the quark number density n_q . These quantities are related by a factor that does not change throughout our study. The baryon number B for N_f degenerate quark flavors is determined by the expression

$$\begin{aligned} B(\theta) &= \frac{1}{N_c} \frac{\partial \ln Z_{GC}}{\partial \theta} \\ &= \frac{N_f}{N_c Z_{GC}} \int \mathcal{D}U e^{-S_G} [\det \Delta(\theta)]^{N_f \text{tr}} \left[\Delta^{-1} \frac{\partial \Delta}{\partial \theta} \right], \end{aligned} \quad (4)$$

where Δ is the lattice Dirac operator. Here and below we omit V and T from the arguments.

We compute $B(\theta)$ numerically in QC₂D at both imaginary and real μ_q . From Eqs. (1),(4) it follows that $B(\theta)$ can be expressed in terms of the normalized canonical partition functions $Z_n = Z_C(nN_c)/Z_C(0)$ as follows:

$$B(\theta) = \frac{2 \sum_{n=1}^{\infty} n Z_n \sinh(nN_c \theta)}{1 + 2 \sum_{n=1}^{\infty} Z_n \cosh(nN_c \theta)} \quad \text{if} \quad \theta_I = 0, \quad (5)$$

$$B(\theta) = \frac{2i \sum_{n=1}^{\infty} n Z_n \sin(nN_c \theta)}{1 + 2 \sum_{n=1}^{\infty} Z_n \cos(nN_c \theta)} \quad \text{if} \quad \theta_R = 0. \quad (6)$$

Our calculations correspond to $N_c = 2$. Where applicable, we do provide the expressions for the general case of arbitrary N_c . Note that Z_n define the probability $\mathcal{Z}(n)$ that a system sampled from the grand-canonical ensemble at $\mu_q = 0$ has the baryon number n , namely $\mathcal{Z}(n) = \frac{Z_{|n|}}{1 + 2 \sum_{k=1}^{\infty} Z_k}$.

The details of our lattice setup are the following. We employ the tree level improved Symanzik gauge action [49] and staggered fermions with the diquark source [24], more details about our lattice action can be found in [37]. We perform simulations on $N_s^3 \times N_t$ lattices at $\beta = 1.7$ and fix the scale using the Sommer parameter value $r_0 = 0.468$ fm. The corresponding lattice spacing is approximately 0.062 fm. We consider $N_s = 28$ which gives lattice size $L \approx 1.74$ fm and a set of temperatures $T = 227, 265, 398$ and 530 MeV corresponding to $N_t = 14, 12, 8$ and 6, respectively. The diquark source coupling $\lambda = 0.00125$ used in our study is much smaller than the quark mass in lattice units $am_q = 0.0125$. However, the corresponding pion mass is rather large, $m_\pi \approx 800$ MeV. We perform our simulations at imaginary quark chemical potential over the range $0 < \theta_I < \pi/2$ and at real quark chemical potential over the range $0 < \mu_q < 600$ MeV.

In this study we explore the cases $T < T_{RW}$ and $T > T_{RW}$ separately, where T_{RW} is the Roberge–Weiss temperature [48]. The former case is referred to as “low temperatures” and the latter—“high temperatures”.

III. ANALYTIC CONTINUATION OF THE QUARK NUMBER DENSITY: LOW TEMPERATURES

Let us first consider a naive analytic continuation procedure by directly utilizing the fugacity expansion of the baryon number. At purely imaginary $\theta = i\theta_I$ this expansion has the form of a trigonometric Fourier series:

$$-iB(\theta)\Big|_{\theta_R=0} \equiv \tilde{B}(\theta_I) = \sum_{n=1}^{\infty} a_n \sin(2n\theta_I), \quad \text{Re } \mu_q = 0. \quad (7)$$

By fitting the lattice data over the segment $0 \leq \theta_I \leq \frac{\pi}{2}$ one first determines the coefficients a_n of the expansion and then inserts the obtained values into the fugacity expansion

$$B(\theta)\Big|_{\theta_I=0} = \sum_{n=1}^{\infty} a_n \sinh(2n\theta_R), \quad \text{Im } \mu_q = 0, \quad (8)$$

which is assumed to describe the baryon number at real values of the chemical potential. However, there exists a problem of convergence. More precisely, if the limit

$$\lim_{n \rightarrow \infty} \frac{|a_{n+1}|}{|a_n|} = j \quad (9)$$

exists and $0 < j < 1$, then the series (8) converges in a finite region

$$|\theta_R| < \frac{-\ln j}{2}. \quad (10)$$

$j = 1$ corresponds to vanishing radius of convergence of the series (8) while for $j \rightarrow 0$ it tends to infinity. In practice, the radius of convergence may be rather small, and in such a case this analytic continuation procedure loses practical relevance. This motivates one to search for a different method of analytic continuation.

A. Determination of Z_n from a direct fit to data

One natural method for $T < T_{RW}$ is to use expressions (5) and (6). The series both in the numerator and the denominator of these expressions converge because Z_n decrease more rapidly than the geometric progression (see [18] for an explicit demonstration). In this case, the right-hand sides in Eqs. (5) and (6) define the density in the entire complex plane of θ . The difficulty lies in the evaluation of a sufficient number of Z_n using a limited lattice data set. As shown below, our data allows to compute only very few of the leading Z_n .

The results of the fit of the imaginary chemical potential data by the function

$$\tilde{B}_N^{(Z)}(\theta_I) = \frac{2 \sum_{n=1}^N n Z_n \sin(2n\theta_I)}{1 + 2 \sum_{n=1}^N Z_n \cos(2n\theta_I)}, \quad \theta_I \in \left[0, \frac{\pi}{2}\right], \quad (11)$$

inspired by the expansion (6), are presented in Tables I and II for temperatures $T = 227$ MeV and $T = 265$ MeV, respectively. Various values of N have been utilized in the fitting procedure, which has been performed using

N	χ^2/N_{dof} and p -value for fit (12)	χ^2/N_{dof} and p -value for fit (11)	a_n	Z_n
2	$\chi^2/N_{dof}=1.66$ $p = 0.069$	$\chi^2/N_{dof} = 47$ $p = 0$	$a_1 = 1.928(38)$ $a_2 = -0.164(31)$	— —
3	$\chi^2/N_{dof}=1.57$ $p = 0.10$	$\chi^2/N_{dof} = 2.21$ $p = 0.012$	$a_1 = 1.917(39)$ $a_2 = -0.128(41)$ $a_3 = -0.036(28)$	$Z_1 = 0.6694(58)$ $Z_2 = 0.2506(50)$ $Z_3 = 0.0510(30)$
4	$\chi^2/N_{dof}=1.71$ $p = 0.072$	$\chi^2/N_{dof}=1.27$ $p = 0.24$	$a_1 = 1.918(40)$ $a_2 = -0.127(41)$ $a_3 = -0.046(44)$ $a_4 = 0.011(35)$	$Z_1 = 0.6709(45)$ $Z_2 = 0.2553(49)$ $Z_3 = 0.0580(33)$ $Z_4 = 0.0049(16)$
5	$\chi^2/N_{dof}=1.09$ $p = 0.36$	$\chi^2/N_{dof}=1.37$ $p = 0.19$	$a_1 = 1.918(32)$ $a_2 = -0.139(33)$ $a_3 = -0.025(36)$ $a_4 = -0.048(34)$ $a_5 = 0.067(25)$	$Z_1 = 0.6708(46)$ $Z_2 = 0.2551(51)$ $Z_3 = 0.0582(34)$ $Z_4 = 0.0057(22)$ $Z_5 = 0.0007(12)$

TABLE I: The coefficients a_n for the fit function (12) and Z_n for the fit function (11) determined from the fits to our data at $T = 227$ MeV over the range $0 \leq \theta_I \leq \frac{\pi}{2}$. We compare results for four values of N in Eqs. (12) and (11). Here we do not show Z_6 and Z_7 , see Table IV for more details. In the second and third columns the respective parameters characterizing goodness-of-fit are indicated.

χ^2/N_{dof} and p -value for fit (12)	χ^2/N_{dof} and p -value for fit (11)	a_n	Z_n
$N = 5$ $\chi^2/N_{dof}=1.76$ $p = 0.061$	$N = 9$ $\chi^2/N_{dof} = 3.21$ $p = 0.0037$	$a_1 = 5.026(66)$ $a_2 = -1.134(77)$ $a_3 = 0.378(80)$ $a_4 = -0.123(74)$ $a_5 = 0.194(104)$	$Z_1 = 0.861288(31)$ $Z_2 = 0.55381(12)$ $Z_3 = 0.269754(13)$ $Z_4 = 0.10131(28)$ $Z_5 = 0.02990(17)$ $Z_6 = 0.00704(39)$ $Z_7 = 0.00133(72)$ $Z_8 = 0.00021(55)$ $Z_9 = 0.00003(21)$
$N = 6$ $\chi^2/N_{dof}=1.92$ $p = 0.045$	$N = 10$ $\chi^2/N_{dof} = 3.68$ $p = 0.0025$	$a_1 = 5.044(79)$ $a_2 = -1.138(81)$ $a_3 = 0.355(98)$ $a_4 = -0.19(17)$ $a_5 = 0.014(16)$ $a_6 = -0.09(20)$	$Z_1 = 0.861288(78)$ $Z_2 = 0.55380(13)$ $Z_3 = 0.269757(22)$ $Z_4 = 0.10134(32)$ $Z_5 = 0.02992(19)$ $Z_6 = 0.00704(65)$ $Z_7 = 0.0013(18)$ $Z_8 = 0.0002(22)$ $Z_9 = 0.00003(170)$ $Z_{10} = 0.000003(560)$

TABLE II: Same as in Table I but for $T = 265$ MeV and different values of N in Eqs. (12) and (11).

gnuplot. The results indicate that our data allow to compute reliably (i.e. fit quality is acceptable and the estimated parameters are stable with respect to change of N) the six leading $Z_1 \div Z_6$. We found that determination of Z_n via the fitting procedure is not a straightforward matter. For instance, the initial values of the fitting parameters in **gnuplot** must be very close to their final values in order to make the fitting algorithm properly convergent [59]. Therefore, for a proper estimation of these parameters one has to know them beforehand fairly accurately. To deal with this problem, we use the following procedure. First we find the Fourier coefficients a_n by performing a fit to the function

$$\tilde{B}_N^{(a)}(\theta_I) = \sum_{n=1}^N a_n \sin(2n\theta_I), \quad \theta_I \in \left[0, \frac{\pi}{2}\right] \quad (12)$$

with an appropriate value of N . Then Z_n are computed using the relation

$$\sum_{n=1}^{\infty} a_n \sin(2n\theta_I) = \frac{2 \sum_{n=1}^{\infty} n Z_n \sin(2n\theta_I)}{1 + 2 \sum_{n=1}^{\infty} Z_n \cos(2n\theta_I)} \quad (13)$$

(see Eqs. (23)-(24) below and text around them for more details) [60]. We use the calculated values of Z_n as the input parameters for the fitting to function (11).

A comment should be made on the range of variation of the cutoff parameter N in computation of Z_n using the above procedure. The procedure is feasible only for some range of N values, which is different for $T = 265$ MeV and $T = 227$ MeV. At $T = 227$ MeV (see Table I) a reliable determination of Z_n using our data is possible when $3 \leq N \leq 7$, whereas at $T = 265$ MeV (see Table II) it is possible only when $9 \leq N \leq 10$. The lower limit on N is associated with behavior of the quark density in the complex fugacity plane near the unit circle. At $T = 265$ MeV, the Lee-Yang zeroes, which restrict the domain of analyticity of $B(\theta)$, are located much closer to the unit circle than at $T = 227$ MeV, hence requiring a larger minimum value of N to obtain reliable results. A similar behavior associated with the Lee-Yang zeroes has been observed in the earlier studies of Ref. [55]. As for the upper value of N , the direct fits for $N > 7$ at $T = 227$ MeV and for $N > 10$ at $T = 265$ MeV are hindered by insufficient statistics.

B. Model-dependent fit functions

Another way to perform the analytic continuation is through the use of model-dependent fit functions. The advantage is that in such a case one only has to fix a few model parameters, which is feasible to do using the available lattice data. One can then calculate as many coefficients a_n as needed to determine both the Z_n and the behavior of the baryon number at real chemical potentials. The disadvantage here is the necessity to rely on model assumptions.

We consider two models which have recently been discussed in the literature in the context of full QCD: the cluster expansion model (CEM) [50] and the rational function model (RFM) [51], each containing two free parameters.

Let us consider the CEM first. We will use the notation a_n^{CEM} for the Fourier coefficients a_n in Eq. (7) computed in the framework of the CEM. The CEM fixes all higher-order Fourier coefficients a_n^{CEM} at $n \geq 3$ as function of the leading two. This is done in such a way as to reproduce the Stefan-Boltzmann limit of a free quark gas when the input leading two coefficients coincide with the Stefan-Boltzmann limiting values. In Ref. [50] the CEM was formulated for $N_c = 3$ QCD with 2+1 flavors, and was applied to imaginary μ_B lattice QCD data [52] at physical quark masses. Here we adopt the CEM for QC₂D with two flavors, as appropriate for our lattice simulations. The CEM coefficients can be represented in terms of two free parameters b and q (instead of b_1 and b_2 used in Refs. [50, 52]), which for the two-flavor QCD read as:

$$a_n^{\text{CEM}} = (-1)^{n+1} \frac{b q^{n-1}}{n} \left[1 + \frac{6}{\pi^2(N_c^2 - 1)n^2} \right], \quad (14)$$

where

$$b = \frac{b_1 \pi^2 (N_c^2 - 1)}{6 + (N_c^2 - 1) \pi^2}, \quad q = -\frac{4(6 + \pi^2(N_c^2 - 1))}{3 + 2\pi^2(N_c^2 - 1)} \frac{b_2}{b_1}. \quad (15)$$

The RFM is similar to CEM in that it also employs the leading two Fourier coefficients to fix all other coefficients and it matches the Stefan-Boltzmann limit of massless quarks. However, in contrast to the CEM where the Fourier coefficients exhibit exponential scaling at large n , in the RFM they obey a power-law scaling. In what follows, the coefficients a_n in Eq. (7) derived in the RFM are designated by a_n^{RFM} . They can be represented in terms of two parameters d and κ via a concise formula

$$a_n^{\text{RFM}} = (-1)^{n+1} d \frac{1 + \frac{\pi^2(N_c^2 - 1)}{6} n^2}{n^3(1 + n\kappa)}. \quad (16)$$

Inserting expressions (14) or (16) into (12) and performing the respective fit over the range $\theta_I \in [0, \pi/2]$ at some particular value of N , we extract the CEM parameters b and q or the RFM parameters d and κ from our data and thus determine all coefficients a_n^{CEM} or a_n^{RFM} making it possible to find Z_n^{CEM} or Z_n^{RFM} .

The results of this procedure are presented in Table III. We choose the cutoff parameter N in (12) as $N = 12$ in the case of CEM and $N = 20$ in the case of RFM finding that the results of the fitting procedure depend only weakly on N as it takes greater values[61].

The p values listed in Table III indicate that the CEM fits our data at imaginary chemical potential substantially better than the RFM.

T , MeV	CEM				RFM			
	p -value	b	q	r_{bq}	p -value	d	κ	$r_{d\kappa}$
227	0.022	1.596(34)	0.200(46)	0.672	0.004	-0.128(56)	-1.40(17)	0.9990
265	0.063	4.209(50)	0.520(28)	0.735	0.005	6.1(4.6)	6.1(5.4)	0.9995

TABLE III: Parameters b and q of the CEM and d and κ of the RFM determined from the fit to our data over the range $0 \leq \theta_I \leq \frac{\pi}{2}$, the correlations r_{bq} between b and q and $r_{d\kappa}$ between d and κ are also shown.

The Fourier coefficients a_n^{CEM} and a_n^{RFM} related to the CEM and RFM models, respectively, are presented in Table IV (for $T = 227$ MeV) and in Table V (for $T = 265$ MeV). Their errors are evaluated by propagating the fit errors of two correlated parameters b and q (d and κ in case of RFM), e.g for a_n^{CEM} one has

$$\sigma^2(a_n^{\text{CEM}}) = \sigma_b^2 \left(\frac{\partial a_n^{\text{CEM}}}{\partial b} \right)^2 + 2\sigma_b\sigma_q r_{bq} \left(\frac{\partial a_n^{\text{CEM}}}{\partial b} \right) \left(\frac{\partial a_n^{\text{CEM}}}{\partial q} \right) + \sigma_q^2 \left(\frac{\partial a_n^{\text{CEM}}}{\partial q} \right)^2, \quad (17)$$

where $\sigma_{b,q}$ are the standard deviations of b and q , r_{bq} is the correlator between the two parameters. The derivatives are calculated using Eq. (14).

n	a_n	a_n^{CEM}	a_n^{RFM}	Z_n	Z_n^{CEM}	Z_n^{RFM}
1	1.918(32)	1.919(42)	1.916(47)	0.6697(45)	0.6686(56)	0.6674(66)
2	-0.139(33)	-0.168(40)	-0.185(47)	0.2527(50)	0.2530(60)	0.2525(74)
3	-0.025(36)	0.022(10)	0.067(19)	0.0562(34)	0.0621(34)	0.0644(35)
4	-0.048(34)	-0.0032(22)	-0.034(10)	0.0059(21)	0.0107(11)	0.0118(10)
5	0.067(25)	0.00051(47)	0.0213(64)	0.0031(19)	0.00137(23)	0.00181(19)
6	—	-0.000085(97)	-0.0143(44)	0.0026(15)	0.000135(34)	0.000154(40)
7	—	0.000015(20)	0.0103(32)	0.00079(86)	0.0000104(37)	0.0000533(52)
8	—	-0.0000026(40)	-0.0078(24)	—	0.00000065(31)	—

TABLE IV: Fourier coefficients and Z_n extracted from the lattice data at $T = 227$ MeV by the direct fit (see also Table I) as well as with use of the CEM and RFM models.

n	a_n	a_n^{CEM}	a_n^{RFM}	Z_n	Z_n^{CEM}	Z_n^{RFM}
1	5.026(66)	5.062(60)	5.06(13)	0.861330(36)	0.86135(122)	0.8626(14)
2	-1.134(77)	-1.150(72)	-1.189(88)	0.553886(121)	0.55392(313)	0.5575(35)
3	0.378(80)	0.388(45)	0.528(50)	0.269786(13)	0.26987(344)	0.2746(39)
4	-0.123(74)	-0.150(25)	-0.298(31)	0.10130(28)	0.10138(230)	0.1053(27)
5	0.194(104)	0.062(14)	0.191(21)	0.02989(17)	0.02989(107)	0.0320(13)
6	—	-0.0269(74)	-0.133(15)	0.00704(39)	0.00703(37)	0.00789(48)
7	—	0.0120(39)	0.098(12)	0.00133(72)	0.001338(95)	0.00160(14)
8	—	-0.0054(21)	-0.0752(92)	< 0.0006	0.000209(20)	0.000270(31)
9	—	0.0025(11)	0.0595(74)	< 0.0002	0.0000270(32)	0.0000387(56)

TABLE V: Same as in Table IV but for $T = 265$ MeV.

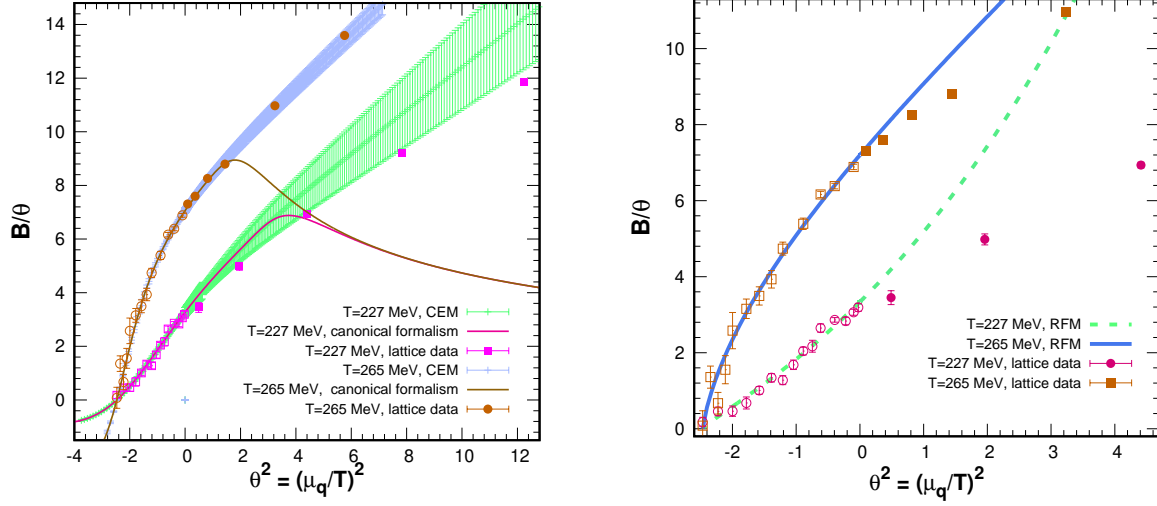


FIG. 1: The lattice results for the ratio B/θ as a function of $\theta^2 = (\mu_q/T)^2$ are compared with the results of the CEM, Eq. (19) (left panel) and RFM, Eq. (22) (right panel) at temperatures $T = 227$ MeV and 265 MeV. The corridors of errors are shown only in the left panel.

C. Analytical continuation of the baryon number to real chemical potentials

On the basis of the above considerations one can naively assume that, at physical values of the quark chemical potential, the expectation value of the baryon number in the lattice volume can be given by the limit

$$B^{(a)}(\theta_R) = \lim_{N \rightarrow \infty} B_N^{(a)}(\theta_R) \equiv \lim_{N \rightarrow \infty} \sum_{n=1}^N a_n \sinh(2n\theta_R) , \quad (18)$$

where this limit exists. The truncated series $B_N^{(a)}(\theta)$ can be used for analytical continuation provided that the whole series converges. However, the Fourier coefficients $a_n^{\text{CEM}}, a_n^{\text{RFM}}$ calculated in the models under consideration, do not decrease sufficiently fast for the series (18) to converge in the whole range of relevant chemical potential values. The power-like decrease of a_n^{RFM} implies zero radius of convergence of (18) in θ plane, therefore, the baryon number parameterised in the RFM cannot be continued to physical values of θ using partial sums of the series (18). In case of the CEM the series (18) converges at $|\theta| < \frac{-\ln q}{2}$. Such a small radius of

convergence gives rise to a dramatic deviation of a partial sum $B_N^{(a)}(\theta)$ from the numerically calculated values of the baryon number already at rather small values of θ_R , see Fig. 3 below.

Fortunately, the series (7) can be summed up analytically in both CEM and RFM cases, which can be used to perform the analytic continuation for the entire complex plane of θ . We shall refer to this analytic continuation procedure presented in this subsection as "direct" to distinguish from the method based on the coefficients Z_n , presented in the next subsection.

The summation was first presented in [53] for the CEM, here we rewrite it as an analytic function of the complex variable θ using the parameters b and q for QCD with N_f quark flavors and N_c colors:

$$B_{\text{CEM}}(\theta) = \frac{b}{2q} \left\{ \ln \frac{1 + q \exp(\theta N_c)}{1 + q \exp(-\theta N_c)} + \frac{6}{\pi^2(N_c^2 - 1)} \left[\text{Li}_3(-q e^{-\theta N_c}) - \text{Li}_3(-q e^{\theta N_c}) \right] \right\} . \quad (19)$$

In the limit of free massless N_f quark flavors one has $q = 1$ and

$$b = \frac{2}{3} \frac{N_f(N_c^2 - 1)}{N_c^3} \frac{N_s^3}{N_t^3} , \quad (20)$$

and Eq. (19) reduces to the baryon number of a free quark gas. As illustrated in the left panel of Fig. 1, the function (19) adequately describes our lattice data at both imaginary and real values of θ after we determine the parameters b and q fitting our data at imaginary θ . The corridor of errors is determined from the condition that the function (19) at each particular value of θ is considered as the function of two correlated random variables b and q ; in so doing, we employ the formula analogous to (17).

At $\theta = i\theta_I$, the function (19) is well approximated by the truncated Fourier series (12) for sufficiently large $N \sim 10 \div 20$, therefore, the CEM results shown in Tables IV and V can be obtained using of the Eqs. (19) or (12).

We see a very good agreement of the baryon number calculated at positive values of θ^2 using CEM with the lattice data, for both $T = 227$ MeV and $T = 265$ MeV and over the full range of the explored chemical potentials. This range covers $0 < \mu_q/T < 3.5$ or $0 < \mu_q < 800$ MeV for $T = 227$ MeV and $0 < \mu_q/T < 2.4$ or $0 < \mu_q < 640$ MeV for $T = 265$ MeV. It is important to extend this analysis to other values of T in order to understand whether such agreement between the CEM and lattice data is common to all $T < T_{RW}$.

We also perform the summation of the Fourier series in the RFM. This summation, which has not been presented in the prior literature, has the form

$$-iB(\theta)\Big|_{\theta_R=0} = d \left\{ \left(\frac{\pi^2(N_c^2 - 1)}{6} + \kappa^2 \right) \left[\frac{\theta_I N_c}{2} - \left(\beta \left(\frac{1}{\kappa} \right) - \frac{\kappa}{2} \right) \sin \left(\frac{\theta_I N_c}{\kappa} \right) \right. \right. \\ \left. \left. - \frac{1}{2} \int_0^{\theta_I N_c} dt \tan \frac{t}{2} \sin \frac{\theta_I N_c - t}{\kappa} \right] + \frac{\pi^2}{12} \left(\theta_I N_c - \frac{(\theta_I N_c)^3}{\pi^2} \right) - \kappa \int_0^{\theta_I N_c} \ln \left(2 \cos \frac{t}{2} \right) dt \right\} \quad (21)$$

where $\beta(z) = \frac{1}{2} \left(\psi \left(\frac{z+1}{2} \right) - \psi \left(\frac{z}{2} \right) \right)$ and $\psi(z) = \frac{1}{\Gamma(z)} \frac{d\Gamma(z)}{dz}$ is the logarithmic derivative of the Gamma function $\Gamma(z)$. The limit of free massless quarks with N_c colors is approached when $\kappa = 0$ and $d = \frac{4N_f}{\pi^2 N_c^3} \frac{N_s^3}{N_t^3}$.

The above expression represents the imaginary part of the function

$$B_{RFM}(\theta) = d \left\{ \left(\frac{\pi^2(N_c^2 - 1)}{6} + \kappa^2 \right) \left[\frac{\theta N_c}{2} - \left(\beta \left(\frac{1}{\kappa} \right) - \frac{\kappa}{2} \right) \sinh \left(\frac{\theta N_c}{\kappa} \right) \right. \right. \\ \left. \left. + \frac{1}{2} \int_0^{\theta N_c} dt \tanh \frac{t}{2} \sinh \frac{\theta N_c - t}{\kappa} \right] + \frac{\pi^2}{12} \left(\theta N_c + \frac{(\theta N_c)^3}{\pi^2} \right) - \kappa \int_0^{\theta N_c} \ln \left(2 \cosh \frac{t}{2} \right) dt \right\} \quad (22)$$

at the imaginary values of θ .

As clearly seen in the right panel of Fig. 1, in contrast to the CEM, the RFM significantly deviates from the lattice data at real θ , even though this function fits the data equally well at imaginary θ . Qualitatively, $B^{RFM}(\theta_R)$ does capture some of the features in the lattice data at $T = 265$ MeV but exhibits essentially different qualitative behavior at $T = 227$ MeV where $B^{RFM}(\theta_R)$ is a strongly convex down function, whereas the data show a slight convexity upwards. Let us note that the function $B_{RFM}(\theta)$ on the imaginary axis involves nonanalyticity of the type $\left(\frac{\pi}{N_c} - \theta_I \right) \ln \left(\frac{\pi}{N_c} - \theta_I \right)$: its first derivative tends to infinity as $\theta_I \rightarrow \pi/N_c$. This observation is of relevance as it runs contrary to the expectation that the quark density at $T < T_{RW}$ is an analytic function at the θ plane imaginary axis and in its immediate vicinity. This may explain the significant deviations of the RFM from the lattice data at $T < T_{RW}$.

To conclude, the analytic continuation of the quark density to real quark chemical potentials provided by the CEM fits lattice data much better than that provided by the RFM. This observation is similar to the conclusions of Ref. [58] regarding the description of baryon number susceptibilities in (2+1)-flavor QCD, where the CEM was also found to provide a more accurate description of the lattice data.

D. Finding Z_n in CEM and RFM

As was explained above, Z_n can be evaluated using the following procedure: first, we find coefficients a_n either by direct fitting to Eq. (12) or using a model, and second, we use Eq. (13) in order to express Z_n in terms of a_n . Multiplying both sides of Eq. (13) by the denominator of the right hand side and employing trigonometric

identities, we derive the following relations between a_n and Z_n :

$$a_i = \sum_{j=1}^{\infty} W_{ij} Z_j, \quad (23)$$

where

$$W_{jk} = 2j\delta_{jk} - a_{j+k} + a_{|j-k|} \cdot \text{sign}(k-j) \quad [\text{here } \text{sign}(0) = 0]. \quad (24)$$

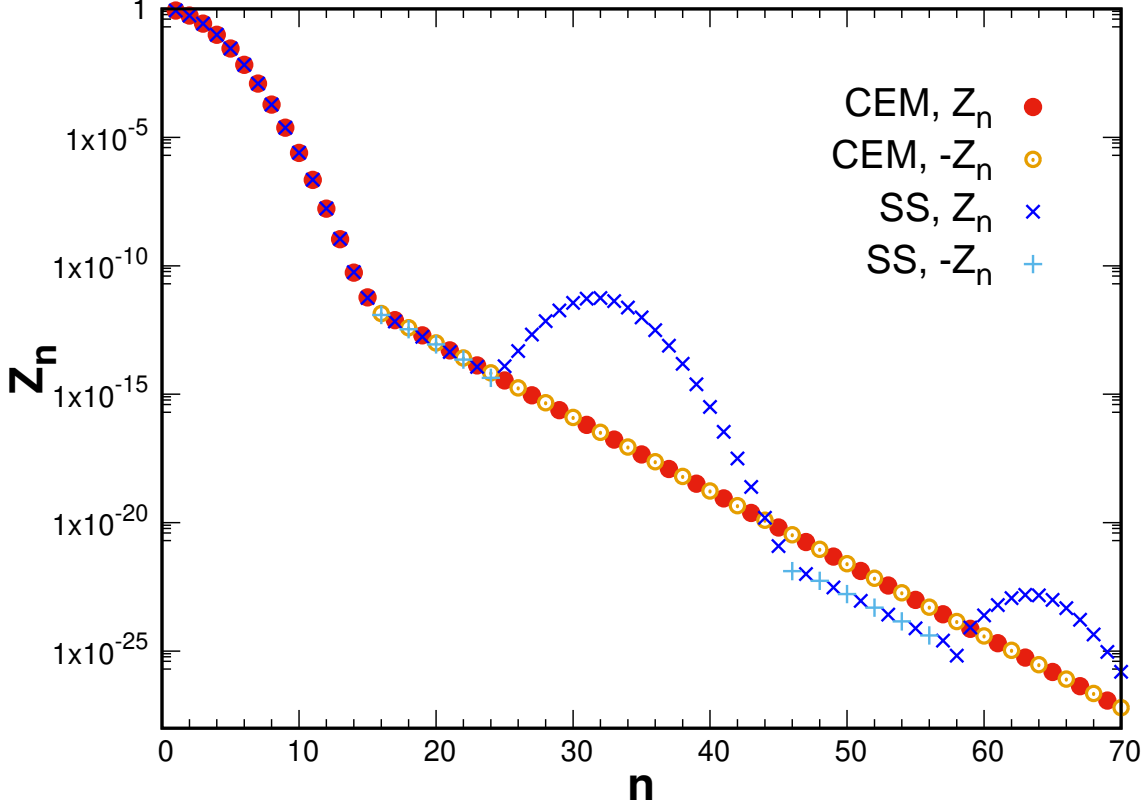


FIG. 2: Behavior of Z_n at $T = 265$ MeV. Shown are the cases when $Z_{GC}(\theta_I, T, V)$ is approximated by Eq. (19) (CEM) and by the truncated series of 31 sines (SS).

As Z_j rapidly decrease with increasing j , we can neglect the terms in this sum starting from some $j = N + 1$. Thus, we arrive at the linear system of N equations for determination of Z_j in terms of a_i . This system can be cast in the matrix form where \mathbf{a} is the column vector of the coefficients a_n and elements of the square matrix \mathbf{W} have the form (24). To find N coefficients Z_n we need $2N$ coefficients a_n because the $N \times N$ matrix \mathbf{W} involves a_i from a range $i = 1, 2, \dots, 2N$.

Alternatively, the coefficients Z_n can also be computed using an integration method discussed in Ref. [18]. If the baryon number is given by Eq. (12) with known Fourier coefficients a_n then

$$Z_{GC}(\theta_I) = \exp \left(-N_c \int_0^{\theta_I} B_N^{(a)}(x) dx \right) = \exp \left(N_c \sum_{n=1}^N \frac{a_n}{2n} \left(\cos(nN_c\theta_I) - 1 \right) \right) \quad (25)$$

and we can use Eq. (2) and the relation $Z_n = Z_C(nN_c)/Z_C(0)$ to evaluate Z_n . This method is somewhat more general, as it does not necessarily relies on the truncation of the series, but can be performed if the baryon

number as function of θ_I is known explicitly. The comparisons between the two methods also provide a cross-check of the accuracy of Z_n determination. As we noted above, the results obtained by these two methods coincide for up to 10 ÷ 20 significant digits.

The obtained Z_n are then used to determine the functions

$$B_N^{(Z)}(\theta) = \frac{2 \sum_{n=1}^N n Z_n \sinh(2n\theta)}{1 + 2 \sum_{n=1}^N Z_n \cosh(2n\theta)} \quad (26)$$

providing an approximation to $B(\theta)$ at real μ_q .

Figure 2 depicts the behavior of Z_n in the CEM for $T = 265$ MeV which has been obtained using the integration method. Calculations have been performed in two different ways. In the first case, we used the summed baryon number from the CEM given in Eq. (19) to evaluate $Z_{GC}(\theta_I)$ from Eq. (25). In the second case, we approximated the baryon number by a truncated series of sines (SS):

$$B_N^{CEM}(\theta_I) = \sum_{n=1}^N a_n^{CEM} \sin(2n\theta_I)$$

with $N = 21$ and a_n^{CEM} given by (14).

We find that the results between the two cases agree with each other for sufficiently small $n \leq 22$. Differences occur at larger n which are attributed to the artefact of using truncated series of sines. From the physics point of view, Z_n exhibit regular behavior at $n \leq 15$, where they are all positive. However, at $n \geq 16$ negative values of Z_n are obtained which is unphysical. On one hand, this may indicate that Z_n at large n are sensitive to subtle physical effects not captured by the CEM. On the other hand, the determination of Z_n at large n may also be sensitive to the finite volume effects, whereas the thermodynamic limit is implicitly assumed in the CEM. For $T = 227$ MeV a qualitatively similar behavior of Z_n is observed.

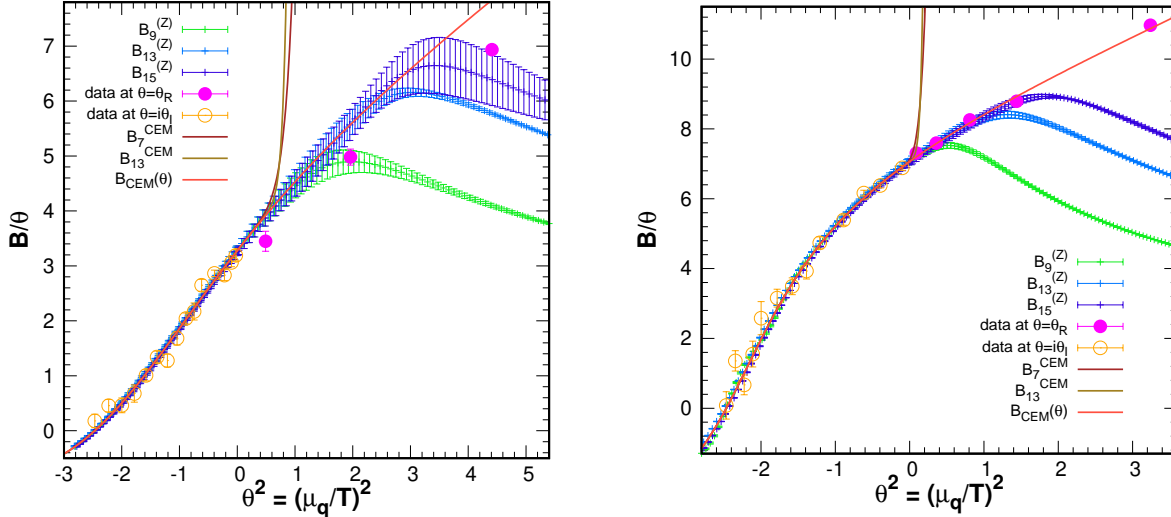


FIG. 3: The functions $B_N^{CEM}(\theta)$ and $B_N^{(Z)}(\theta)$ obtained in the CEM at various N are plotted versus θ^2 at $T = 227$ MeV (left panel) and $T = 265$ MeV (right panel).

The expectation value of the baryon number in the lattice volume at physical values of the quark chemical potential can be obtained not only by the “direct” analytic continuation described in the previous subsection, but also through the use of Z_n via the formula (see Sec. II)

$$B^{(Z)}(\theta_R) = \lim_{N \rightarrow \infty} B_N^{(Z)}(\theta_R) \equiv \lim_{N \rightarrow \infty} \frac{2 \sum_{n=1}^N n Z_n \sinh(2n\theta_R)}{1 + 2 \sum_{n=1}^N Z_n \cosh(2n\theta_R)}. \quad (27)$$

In Fig. 3 we compare the functions

$$\frac{1}{\theta} B_N^{CEM}(\theta) = \frac{1}{\theta} \sum_{n=1}^N a_n^{CEM} \sinh(\theta) = \begin{cases} \frac{1}{\theta_R} \sum_{n=1}^N a_n^{CEM} \sinh(\theta_R) & \text{if } \theta_I = 0 \\ \frac{1}{\theta_I} \sum_{n=1}^N a_n^{CEM} \sin(\theta_I) & \text{if } \theta_R = 0 \end{cases}$$

and

$$\frac{1}{\theta} B_N^{(Z)}(\theta) = \frac{1}{\theta} \frac{2 \sum_{n=1}^N n Z_n \sinh(2n\theta)}{1 + 2 \sum_{n=1}^N Z_n \cosh(2n\theta)} = \begin{cases} \frac{1}{\theta_R} \frac{2 \sum_{n=1}^N n Z_n \sinh(2n\theta_R)}{1 + 2 \sum_{n=1}^N Z_n \cosh(2n\theta_R)} & \text{if } \theta_I = 0 \\ \frac{1}{\theta_I} \frac{2 \sum_{n=1}^N n Z_n \sin(2n\theta_I)}{1 + 2 \sum_{n=1}^N Z_n \cos(2n\theta_I)} & \text{if } \theta_R = 0 \end{cases}$$

obtained in the CEM at various N . At both temperatures we see that both $B_7^{CEM}(\theta)$ and $B_{13}^{CEM}(\theta)$ depart from the line of lattice data dramatically at real θ starting from a small value θ_R ($\theta_R^2 \sim 0.6$ for $T = 227$ MeV and $\theta_R^2 \sim 0.12$ for $T = 265$ MeV). The point is that the series

$$\sum_{n=1}^{\infty} a_n^{CEM} \sinh(2n\theta) \quad (28)$$

diverges at real $\theta > -\frac{\ln(q)}{2} \approx 0.81$ at $T = 227$ MeV and $\theta > 0.33$ at $T = 265$ MeV, as it follows from formulas (14) and (10).

As one can see from Fig. 3 fit-functions $B_N^{(Z)}(\theta)$ approximate well the lattice data over a broad range of θ_R and this range increases with N . However, there exists a maximum value of $N = N_{max}$ such that Z_n at $n > N_{max}$ are not properly extracted from the data, which is indicated by alternating sign and a slow decrease of the absolute value of Z_n at $n > N_{max}$ as was shown in Fig. 2. The values of N_{max} and the corresponding ranges of $\theta_R = \mu_q/T$ are as follows:

- $|\theta| < 1.7$ ($|\mu_q| < 380$ MeV) at $N = N_{max} = 15$ for $T = 227$ MeV,
- $|\theta| < 1.2$ ($|\mu_q| < 320$ MeV) at $N = N_{max} = 15$ for $T = 265$ MeV.

Since N_{max} values specified here give the upper bounds on the ranges of values of n where all Z_n computed for the CEM are positive we consider the respective values of μ_q/T as the upper bounds on the domain of μ_q/T where the corrections to the CEM can be neglected.

As it follows from the previous subsection, the "direct" analytical continuation provided by the CEM agrees with lattice data in a wider range than the analytical continuation based on the grand canonical approach. However, we believe that the domain of θ_R in which the latter continuation provides a good agreement with the data expands with increasing N_{max} and if sufficiently large values of N_{max} were available on a lattice of a given size, the analytical continuation based on the grand canonical approach would work just as well as the "direct" analytical continuation. Moreover, for a reasonable comparison of these two methods of analytical continuation one has to explain both the abrupt change of the n -dependence of Z_n at $n = N_{max}$ shown in Fig. 2 as well as the appearance of unphysical negative values of Z_n . The respective critical number N_{max} is associated with a particular quark density ρ_c , so we conclude that at $\rho < \rho_c$ both methods are valid. It should be emphasized that the method based on the grand canonical approach is model independent and stems from first principles. Therewith, the very existence of ρ_c as well as its estimates in various models is not properly understood and may be the subject of future work. Here we only assume that it is connected with finite-volume effects and/or significant corrections to the models under consideration at high densities.

The continuation of the Fourier series in RFM to real values of θ is more subtle. This series

$$\sum_{n=1}^{\infty} a_n^{RFM} \sinh(2n\theta) \quad (29)$$

(analogous to the series (28) in CEM) diverges at all real $\theta \neq 0$ because of only power-like decrease of a_n^{RFM} with n .

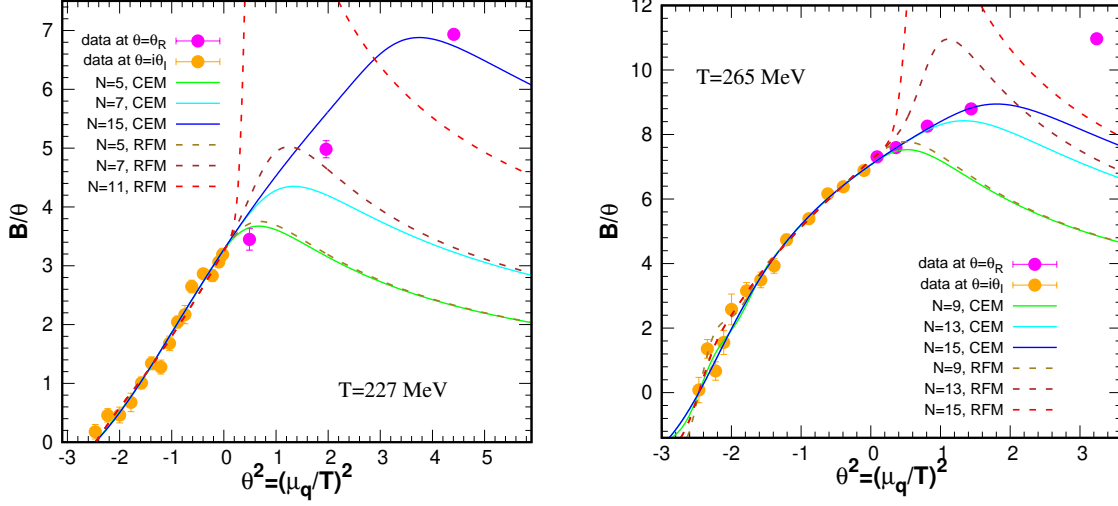


FIG. 4: The functions $B_N^{(Z)}$ obtained in the CEM (solid lines) are compared with those obtained in the RFM (dashed lines) at various N : $T = 227$ MeV (left panel) and $T = 265$ MeV (right panel).

In Fig. 4 we compare the quantities $B_N^{(Z)}$ obtained in the CEM with those obtained in the RFM at real values of μ_q ($\theta^2 \geq 0$). We are interested in the range of real μ_q , where the plots of $B_N^{(Z)}$ come close to the line defined by the lattice data. This range extends with an increase of N in the case of CEM and vanishes at all N in the case of RFM. To illustrate the effect of the presence of negative Z_n on the analytic continuation we also show the result in the RFM for $N = 11$ at $T = 227$ MeV, where there is a contribution from negative Z_n .

IV. ANALYTIC CONTINUATION OF THE QUARK NUMBER DENSITY: HIGH TEMPERATURES

At high temperatures ($T > T_{RW}$) the conventional method is to use polynomial fit functions, namely one performs a fit by a polynomial of degree $2N_p - 1$ to data for the baryon number at imaginary values of $\theta = i\theta_I$ and then makes the analytical continuation to real values of θ (see e.g. [18, 56]). In this case N_p determines the number of fit parameters. This number is less than the order of the polynomial $2N_p - 1$ because all even powers vanish due to the CP-symmetry. We analyze two values of temperatures in this regime: $T = 398$ MeV and 530 MeV.

A. Analytical continuation based on power series expansion

Here we fit the baryon number at imaginary chemical potential by the function

$$\tilde{B}(\theta_I) \simeq \sum_{n=1}^{N_p} a_n^{\text{RFM}} (\theta_I)^{2n-1} \quad (30)$$

using the values $N_p = 2, 3, 4$. The fit parameters are a_n^{RFM} and their resulting values are shown in Table VI. Figure 5 depicts the analytic continuation of to the domain of real θ using the values of the extracted fit parameters. The errors in the values of the fit parameters are propagated, taking into accounts their correlated nature, the resulting error in the baryon number is depicted in Fig. 5 by the bands. Comparison with the lattice data at real values of θ indicates that the most accurate analytic continuation is achieved by using a It is seen that the best continuation is provided by polynomial of 5th degree at $T = 530$ MeV and a polynomial of the 3rd degree at $T = 398$ MeV.

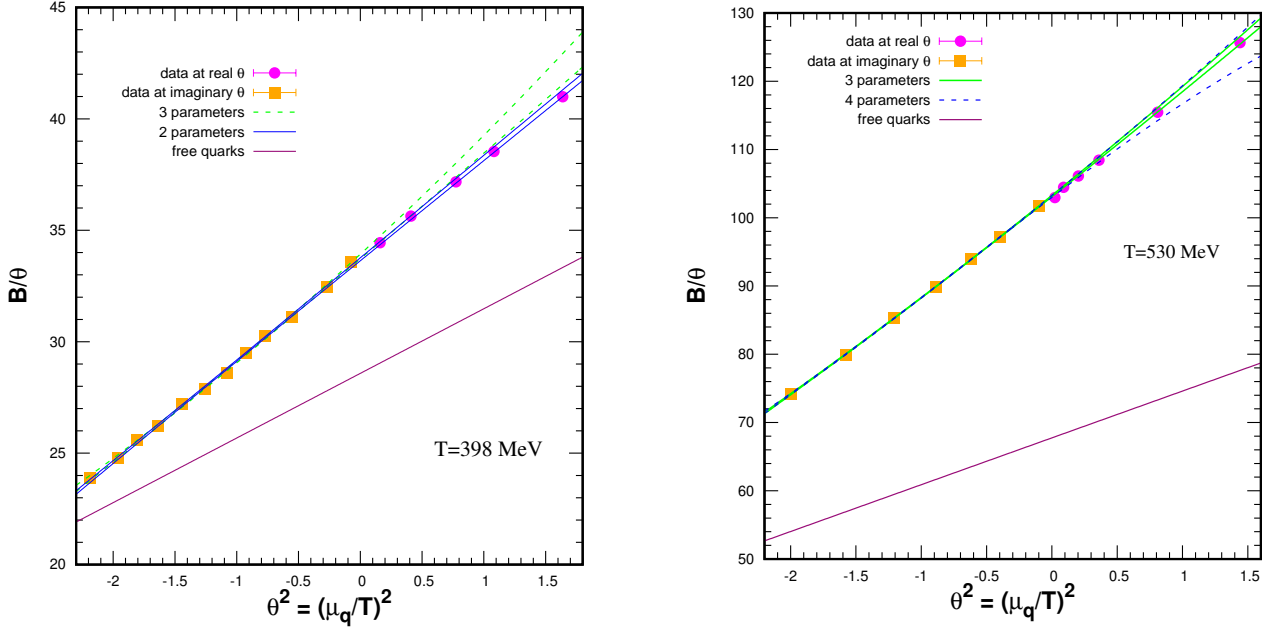


FIG. 5: Analytical continuation of the baryon number from imaginary to real θ with the use of the power fit (30) at $T = 398$ MeV (left panel) and $T = 530$ MeV (right panel). Each pair of similar lines shows the respective corridor of errors.

To establish the role of quark interactions, we compare our results with the baseline of free massless quarks at the same volume and temperature. The partition function in this case has the form

$$Z_{GC}^{(free)}(\theta) = A \exp \left[c \left(\theta^2 + \frac{\theta^4}{2\pi^2} \right) \right] \quad (31)$$

where $c = \frac{g_f VT^3}{12}$ (in the case of lattice QC₂D with two flavors, $c = \frac{2N_s^3}{3N_t^3}$), and $A = \exp \left(\frac{7c\pi^2}{30} \right)$. The baryon number in the lattice volume is determined as $B = \frac{1}{N_c} \frac{\partial \ln Z_{GC}}{\partial \mu_q}$, giving

$$B^{free}(\theta) = c \left(\theta + \frac{\theta^3}{\pi^2} \right). \quad (32)$$

This corresponds to a polynomial of degree 3 ($N_p = 2$) in formula (30), i.e. $B = c_1^{free} \theta + c_2^{free} \theta^3$. The numerical values of the coefficients c_1^{free} and c_2^{free} are shown in Table VI, where they are compared with the results. The resulting behavior of $B^{free}(\theta)$ is shown in Fig. 5.

T (MeV)	N_{param}	χ^2/N_{dof}	c_1	c_2	c_3
398	2	0.83	33.698(66)	4.548(56)	-
398	3	0.64	33.83(10)	4.88(22)	0.155(96)
398	4	0.70	33.86(15)	5.07(55)	0.37(59)
530	2	4.19	102.859(57)	14.467(52)	-
530	3	0.83	103.182(96)	15.29(20)	0.383(91)
530	4	0.97	103.12(14)	14.98(51)	0.03(55)
398	2	free quarks	28.58	2.90	-
530	2	free quarks	67.75	6.86	-

TABLE VI: The results of the fit by the formula (30). c_4 is poorly determined and is not shown. The exact results for the free quarks are given for comparison.

As is seen in Fig. 5, the baryon number in the free quark limit is smaller than that for interacting quarks; that is, the presence of interactions increases the baryon number at given parameters V, T, μ_q . This is notably different

from (2+1)-flavor QCD with physical quark masses, where lattice QCD calculations indicate that the baryon number is suppressed compared to the free quark limit at similar temperatures and chemical potentials [57].

However, in the analysis of our data, the effects of interactions are clearly seen in the coefficients c_1 and c_2 only. The behavior of the coefficient c_3 , which vanishes for the free quarks, is somewhat unexpected. When evaluated by the three-parameter fit (30), it differs from zero at $T = 530$ MeV, whereas its value is consistent with zero within two standard deviations at $T = 398$ MeV. Thus we conclude that much more extensive data are needed to infer the behavior of the coefficients a_n^{RFM} for $n > 2$.

B. Other schemes

Here we explore other possibilities for performing the analytic continuation at $T > T_{\text{RW}}$. We begin with a consideration of the trigonometric Fourier series expansion of the baryon number over the segment $-\frac{\pi}{2} < \theta_I \leq \frac{\pi}{2}$, focusing on $T = 398$ MeV. Here one utilizes the truncated Fourier series

$$\tilde{B} \simeq \sum_{n=1}^{N_p} a_n^{\text{RFM}} \sin(2n\theta_I) . \quad (33)$$

However, the fit quality of the lattice data is unsatisfactory, giving $\frac{\chi^2}{N_{d.o.f.}} > 200$ using N_p as large as $N_p = 8$. The reason is that the quark number density is a discontinuous function of θ_I at the edges of the interval $-\frac{\pi}{2} < \theta_I \leq \frac{\pi}{2}$: this function is well approximated by a low-degree polynomial (30) over this interval and has to be continued by periodicity with the period π outside the interval, resulting in jumps at $\theta_I = \frac{\pi}{2} + \pi n$, $n \in \mathbb{Z}$. As the Fourier series converges very slowly to a discontinuous function, this results in a poor fit quality.

A different possibility is to use the canonical formalism and the associated formula (5), which has been shown to work reasonably well at $T < T_{\text{RW}}$. On the imaginary axis it has the form (6). However, a fit based on this formula also does not give a reasonable result, with p -value less than 10^{-13} . Thus, one has to consider other possibilities.

We observe that the baryon number can be well fitted by the function

$$\tilde{B} \simeq c \sin(w\theta_I) , \quad (34)$$

where c and w are fitting parameters. The fit result for $T = 398$ MeV is $c = 17.987(60)$, $w = 0.9415(43)$, $\frac{\chi^2}{N_{d.o.f.}} = 0.60$ ($p = 0.81$). One can then use this formula to perform the analytic continuation to real values of θ , the result is depicted in Fig. 6.

The analytic continuation based on Eq. (34) yields a reasonable qualitative behavior, but the resulting baryon number overestimates the lattice data at real values of θ . For this reason, we also consider a more involved fit function with three parameters, namely

$$B \simeq \frac{c \sin(w\theta_I)}{1 + \zeta \cos(w\theta_I)} , \quad (35)$$

which is motivated by formulas (34) and (6). It is seen in Fig. 6 that such fit provides a better analytic continuation to the domain of real θ .

The resulting grand partition functions have the form

$$Z_{GC}(\theta) = \exp\left(\frac{2c}{w} \cosh(w\theta)\right) \quad (36)$$

corresponding to the baryon number (34) and

$$Z_{GC}(\theta) = \left(1 + \zeta \cosh(w\theta)\right)^{\frac{2c}{w\zeta}} , \quad (37)$$

the one corresponding to (35). Note that both formulas are valid on the strip $-\frac{\pi}{2} < \theta_I \leq \frac{\pi}{2}$. For θ_I values outside of this strip, these expressions have to be continued using the periodicity in θ_I with a period π , in accordance with the Roberge-Weiss symmetry [48].

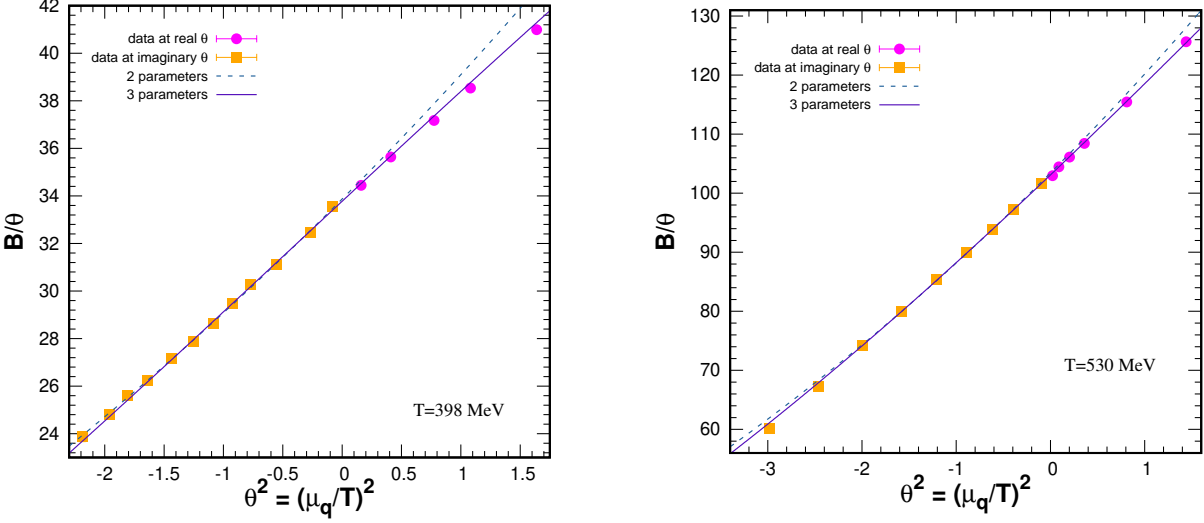


FIG. 6: Two different procedures of analytic continuation are compared: the two-parameter fit is based on formula (34), the three-parameter fit is based on formula (35) associated with the canonical formalism.

Note that the function (37) reduces to (36) in the limit $\zeta \rightarrow 0$. In the case under consideration, this parameter is rather small (see Table VII). However, it is also non-negligible and needed to describe the lattice data at $T = 398$ MeV.

T (MeV)	χ^2/N_{dof}	c	ζ	w
398	0.64	17.89(16)	0.030(43)	0.973(47)
530	0.79	53.21(15)	0.053(13)	1.020(14)

TABLE VII: The results of the fit by the formula (35).

It is seen in Table VII that the values of the parameter w in the argument of the trigonometric functions are close to unity. For this reason, one can enforce the value of w to unity and perform the fitting using the formula

$$\tilde{B} \simeq \frac{c \sin(\theta_I)}{1 + \zeta \cos(\theta_I)} . \quad (38)$$

The results are shown in Table VIII. Goodness-of-fit is excellent, with $\chi^2/N_{dof} \lesssim 1$, and the parameters are determined well. The analytical continuation using this formula fits well the data at real θ , as seen in Fig. 7. Therefore, at high T both the fit by a polynomial [Eq. (30)] and by using trigonometric functions [e.g. Eq. (38)] can be used equally well for the analytic continuation to real values of θ .

It is interesting to note that the fit function (38) can be continued by analyticity to a 2π -periodic in θ_I function associated with a particular Polyakov-loop sector in the Roberge-Weiss approach. The respective partition function, which is given by formula (37) with $w = 1$, provides an interesting toy model at $\frac{2c}{\zeta} = n \in \mathbb{Z}$, which possesses two high-order Lee-Yang zeroes. This can be an interesting subject of future studies.

V. CONCLUSIONS

We have studied the properties of quark number density n_q at real and imaginary values of the quark chemical potential μ_q in QC₂D over the temperature range $230 \text{ MeV} < T < 530 \text{ MeV}$. The analysis utilized the numerical lattice QCD results at both real and imaginary chemical potential, and has been focused on the performance

T (MeV)	χ^2/N_{dof}	c	ζ
398	0.60	17.800(42)	0.0536(39)
530	0.95	53.413(49)	0.0345(15)

TABLE VIII: The results of the fit by the formula (38).

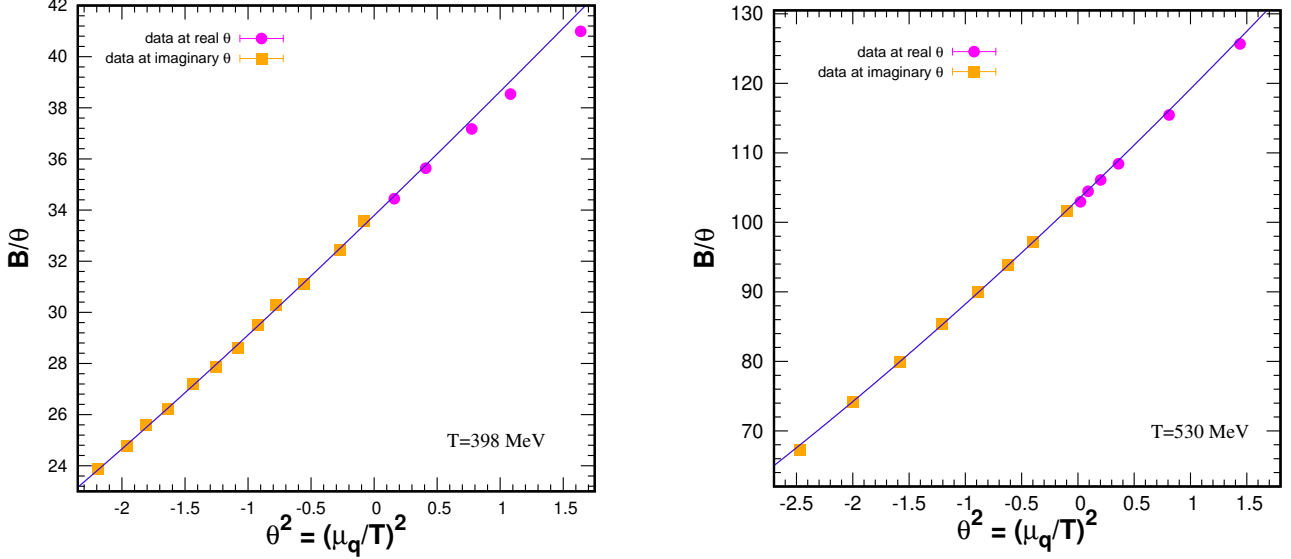


FIG. 7: The results of analytical continuation by formula (38).

of various methods of analytic continuation from imaginary to real chemical potential. This analysis should be useful for the case of full QCD, where the lattice simulations are hindered by the sign problem at real chemical potentials but remain feasible at imaginary chemical potentials. The analysis is focused separately on temperatures below the Roberge-Weiss transition at $T_{RW} \sim 270$ MeV and above.

At low temperatures ($T < T_{RW}$), we first considered the analysis using model-independent expressions, such as the truncated trigonometric series expansion of the baryon number at imaginary chemical potentials [Eq. (12)] or the expression Eq. (11) based on the canonical formalism. These analyses showed limited success, mainly due to insufficient precision of the data that do not yet allow to determine the high-order expansion coefficients reliably.

To proceed further, we then used fit functions based on two phenomenological models that have recently been proposed in the literature, the cluster expansion model (CEM) and the rational function model (RFM). Both of these models make it possible to express all coefficients of the Fourier series for the quark density on the imaginary chemical potential segment $-\frac{\pi}{2} \leq \theta_I \leq \frac{\pi}{2}$ ($\theta_R = 0$) in terms of two parameters that are readily determined by fitting. Moreover, the functions (19) and (22) obtained by summation of these Fourier series for the CEM and the RFM, respectively, readily provide an analytical continuation of the quark density to the real values of θ . While both the CEM and RFM describe the lattice data at imaginary θ similarly well, we find that the CEM also demonstrates large range of agreement with our lattice data at real θ whereas the RFM shows significant deviations from the data.

We further used the CEM and RFM to study the behavior of the canonical partition functions Z_n . We find that the positivity of Z_n is broken in both the CEM and RFM for sufficiently high n . This behavior indicates that either corrections to the models, in particular at high quark densities, are required to recover the physical behavior of Z_n , or that finite-volume effects are still substantial and not under control. We have shown, however, that when only a limited number of the coefficients Z_n , $n < N$ based on the CEM model is considered, where they all exhibit physical behavior, then the analytical continuation based on the canonical approach does agree with the lattice data over a finite range $0 \leq \theta_R \leq \theta_R^{(Z)}(N)$, where $\theta_R^{(Z)}(N)$ increases with N . If it becomes possible to reliably determine the higher order coefficients Z_n , it is feasible that the range on the analytical

continuation based on the canonical formalism can be further extended to larger values of θ_R . This will be the subject of a future work. We also plan to extend our study to lower temperatures to cover, in particular, the vicinity of the QCD transition. Finite volume effects should be also studied in future, and we do plan to simulate larger lattices with N_s up to 56, in addition to the present value, $N_s = 28$. An increased statistics of the simulations will also allow us to compute Z_n for higher values of n using the direct fit approach.

For high temperatures ($T > T_{RW}$) we have found that the quark density at imaginary quark chemical potential over the range $0 < \theta_I < \frac{\pi}{2}$ can be equally well approximated either by a polynomial or by a 2π -periodic trigonometric function (38) that can be associated with the density of colored massless free fermions. The analytic continuation to the real values of θ based on either of these fit-functions works equally well at least up to $\mu_q = 600$ MeV.

Acknowledgments

The authors are grateful to V. Braguta and A. Nikolaev for useful discussions. The work was supported by the grant of the Russian Foundation for Basic Research No. 18-02-40130 mega and partially carried out within the state assignment of the Ministry of Science and Higher Education of Russia (Project No. 0657-2020-0015). This work was partially supported by Grants-in-Aid for Scientific Research (Kakenhi), No. 21K03573. Computer simulations were performed on the FEFU GPU cluster Vostok-1, the Central Linux Cluster of the NRC "Kurchatov Institute" - IHEP, the Linux Cluster of the NRC "Kurchatov Institute" - ITEP (Moscow). In addition, we used computer resources of the federal collective usage center Complex for Simulation and Data Processing for Mega-science Facilities at NRC Kurchatov Institute, <http://ckp.nrcki.ru/>. V.V. acknowledges the support through the Feodor Lynen program of the Alexander von Humboldt foundation, the U.S. Department of Energy, Office of Science, Office of Nuclear Physics, under contract number DE-AC02-05CH11231231, and within the framework of the Beam Energy Scan Theory (BEST) Topical Collaboration.

-
- [1] K. Aamodt *et al.* [ALICE], JINST **3** (2008), S08002
 - [2] J. Adams *et al.* [STAR], Nucl. Phys. A **757** (2005), 102-183 [arXiv:nucl-ex/0501009 [nucl-ex]].
 - [3] N. Abgrall *et al.* [NA61], JINST **9**, P06005 (2014) [arXiv:1401.4699 [physics.ins-det]].
 - [4] Y. Aoki, G. Endrodi, Z. Fodor, S. D. Katz and K. K. Szabo, Nature **443**, 675-678 (2006) [arXiv:hep-lat/0611014 [hep-lat]].
 - [5] A. Bzdak, S. Esumi, V. Koch, J. Liao, M. Stephanov and N. Xu, Phys. Rept. **853**, 1-87 (2020) [arXiv:1906.00936 [nucl-th]].
 - [6] J. Adam *et al.* [STAR], Phys. Rev. Lett. **126**, no.9, 092301 (2021) [arXiv:2001.02852 [nucl-ex]].
 - [7] M. Gazdzicki and P. Seyboth, Acta Phys. Polon. B **47**, 1201 (2016) [arXiv:1506.08141 [nucl-ex]].
 - [8] T. Ablyazimov *et al.* [CBM], Eur. Phys. J. A **53** (2017) no.3, 60 [arXiv:1607.01487 [nucl-ex]].
 - [9] A. N. Sissakian *et al.* [NICA], J. Phys. G **36** (2009), 064069
 - [10] R. Bellwied, S. Borsanyi, Z. Fodor, S. D. Katz, A. Pasztor, C. Ratti and K. K. Szabo, Phys. Rev. D **92** (2015) no.11, 114505 [arXiv:1507.04627 [hep-lat]].
 - [11] H. T. Ding, S. Mukherjee, H. Ohno, P. Petreczky and H. P. Schadler, Phys. Rev. D **92** (2015) no.7, 074043 [arXiv:1507.06637 [hep-lat]].
 - [12] A. Bazavov *et al.* [HotQCD], Phys. Lett. B **795** (2019), 15-21 [arXiv:1812.08235 [hep-lat]].
 - [13] A. Bazavov, D. Bollweg, H. T. Ding, P. Enns, J. Goswami, P. Hegde, O. Kaczmarek, F. Karsch, R. Larsen and S. Mukherjee, *et al.* Phys. Rev. D **101** (2020) no.7, 074502 [arXiv:2001.08530 [hep-lat]].
 - [14] M. D'Elia and M. P. Lombardo, Phys. Rev. D **67** (2003), 014505 [arXiv:hep-lat/0209146 [hep-lat]].
 - [15] M. D'Elia and F. Sanfilippo, Phys. Rev. D **80** (2009), 014502 [arXiv:0904.1400 [hep-lat]].
 - [16] C. Bonati, P. de Forcrand, M. D'Elia, O. Philipsen and F. Sanfilippo, Phys. Rev. D **90** (2014) no.7, 074030 [arXiv:1408.5086 [hep-lat]].
 - [17] M. D'Elia, G. Gagliardi and F. Sanfilippo, Phys. Rev. D **95** (2017) no.9, 094503 [arXiv:1611.08285 [hep-lat]].
 - [18] V. G. Bornyakov, D. L. Boyda, V. A. Goy, A. V. Molochkov, A. Nakamura, A. A. Nikolaev and V. I. Zakharov, Phys. Rev. D **95** (2017) no.9, 094506, [arXiv:1611.04229 [hep-lat]].
 - [19] P. Alba, R. Bellwied, S. Borsanyi, Z. Fodor, J. Günther, S. D. Katz, V. Mantovani Sarti, J. Noronha-Hostler, P. Parotto and A. Pasztor, *et al.* Phys. Rev. D **96** (2017) no.3, 034517 [arXiv:1702.01113 [hep-lat]].
 - [20] V. G. Bornyakov, D. L. Boyda, V. A. Goy, H. Iida, A. V. Molochkov, A. Nakamura, A. A. Nikolaev, V. I. Zakharov and M. Wakayama, EPJ Web Conf. **182** (2018), 02017 [arXiv:1712.02830 [hep-lat]].
 - [21] C. Bonati, M. D'Elia, F. Negro, F. Sanfilippo and K. Zambello, Phys. Rev. D **98** (2018) no.5, 054510 [arXiv:1805.02960 [hep-lat]].

- [22] S. Borsanyi, Z. Fodor, J. N. Guenther, S. K. Katz, K. K. Szabo, A. Pasztor, I. Portillo and C. Ratti, JHEP **10** (2018), 205 [arXiv:1805.04445 [hep-lat]].
- [23] A. Nakamura, Phys. Lett. B **149** (1984), 391
- [24] S. Hands, J. B. Kogut, M. P. Lombardo and S. E. Morrison, Nucl. Phys. B **558** (1999), 327-346, [arXiv:hep-lat/9902034 [hep-lat]].
- [25] J. B. Kogut, D. Toublan and D. K. Sinclair, Phys. Lett. B **514** (2001), 77-87, [arXiv:hep-lat/0104010 [hep-lat]].
- [26] J. B. Kogut, D. Toublan and D. K. Sinclair, Nucl. Phys. B **642** (2002), 181-209, [arXiv:hep-lat/0205019 [hep-lat]].
- [27] S. Muroya, A. Nakamura and C. Nonaka, Phys. Lett. B **551** (2003), 305-310 [arXiv:hep-lat/0211010 [hep-lat]].
- [28] P. Giudice and A. Papa, Phys. Rev. D **69** (2004), 094509 [arXiv:hep-lat/0401024 [hep-lat]].
- [29] S. Hands, S. Kim and J. I. Skullerud, Eur. Phys. J. C **48**, 193 (2006) [arXiv:hep-lat/0604004 [hep-lat]].
- [30] P. Cea, L. Cosmai, M. D'Elia and A. Papa, JHEP **02** (2007), 066 [arXiv:hep-lat/0612018 [hep-lat]].
- [31] P. Cea, L. Cosmai, M. D'Elia and A. Papa, Phys. Rev. D **77** (2008), 051501 [arXiv:0712.3755 [hep-lat]].
- [32] P. Cea, L. Cosmai, M. D'Elia, C. Manneschi and A. Papa, Phys. Rev. D **80** (2009), 034501 [arXiv:0905.1292 [hep-lat]].
- [33] S. Cotter, P. Giudice, S. Hands and J. I. Skullerud, Phys. Rev. D **87** (2013) no.3, 034507, [arXiv:1210.4496 [hep-lat]].
- [34] T. Boz, S. Cotter, L. Fister, D. Mehta and J. I. Skullerud, Eur. Phys. J. A **49**, 87 (2013) [arXiv:1303.3223 [hep-lat]].
- [35] V. V. Braguta, E. M. Ilgenfritz, A. Y. Kotov, A. V. Molochkov and A. A. Nikolaev, Phys. Rev. D **94** (2016) no.11, 114510, [arXiv:1605.04090 [hep-lat]].
- [36] L. Holicki, J. Wilhelm, D. Smith, B. Wellegehausen and L. von Smekal, PoS **LATTICE2016** (2017), 052, [arXiv:1701.04664 [hep-lat]].
- [37] V. Bornyakov, V. Braguta, E. M. Ilgenfritz, A. Y. Kotov, A. Molochkov and A. Nikolaev, JHEP **03**, 161 (2018) [arXiv:1711.01869 [hep-lat]].
- [38] T. Boz, O. Hajizadeh, A. Maas and J. I. Skullerud, Phys. Rev. D **99**, no.7, 074514 (2019) [arXiv:1812.08517 [hep-lat]].
- [39] N. Astrakhantsev, V. Bornyakov, V. Braguta, E. M. Ilgenfritz, A. Kotov, A. Nikolaev and A. Rothkopf, JHEP **05**, 171 (2019) [arXiv:1808.06466 [hep-lat]].
- [40] T. Boz, P. Giudice, S. Hands and J. I. Skullerud, Phys. Rev. D **101**, no.7, 074506 (2020) [arXiv:1912.10975 [hep-lat]].
- [41] K. Iida, E. Itou and T. G. Lee, JHEP **01** (2020), 181 [arXiv:1910.07872 [hep-lat]].
- [42] J. Wilhelm, L. Holicki, D. Smith, B. Wellegehausen and L. von Smekal, Phys. Rev. D **100** (2019) no.11, 114507, [arXiv:1910.04495 [hep-lat]].
- [43] V. Bornyakov, V. Braguta, A. Nikolaev and R. Rogalyov, Phys. Rev. D **102** (2020), 114511 [arXiv:2003.00232 [hep-lat]].
- [44] N. Astrakhantsev, V. V. Braguta, E. M. Ilgenfritz, A. Y. Kotov and A. A. Nikolaev, Phys. Rev. D **102** (2020) no.7, 074507 [arXiv:2007.07640 [hep-lat]].
- [45] P. V. Buividovich, D. Smith and L. von Smekal, Phys. Rev. D **102** (2020) no.9, 094510 [arXiv:2007.05639 [hep-lat]].
- [46] K. Iida, E. Itou and T. G. Lee, PTEP **2021** (2021) no.1, 013B05 [arXiv:2008.06322 [hep-lat]].
- [47] A. Hasenfratz and D. Toussaint, Nucl. Phys. B **371** (1992), 539-549
- [48] A. Roberge and N. Weiss, Nucl. Phys. B **275** (1986), 734-745
- [49] P. Weisz, Nucl. Phys. B **212** (1983), 1-17
- [50] V. Vovchenko, J. Steinheimer, O. Philipsen and H. Stoecker, Phys. Rev. D **97** (2018) no.11, 114030, [arXiv:1711.01261 [hep-ph]].
- [51] G. A. Almasi, B. Friman, K. Morita, P. M. Lo, and K. Redlich, Phys. Rev. D **100** (2019) no.1, 016016 [arXiv:1805.04441 [hep-ph]].
- [52] V. Vovchenko, A. Pasztor, Z. Fodor, S. D. Katz, and H. Stoecker, Phys. Lett. B **775** (2017) 71-78, [arXiv:1708.02852 [hep-ph]].
- [53] V. Vovchenko, J. Steinheimer, O. Philipsen, A. Pasztor, Z. Fodor, S. D. Katz and H. Stoecker, Nucl. Phys. A **982** (2019), 859-862 [arXiv:1807.06472 [hep-lat]].
- [54] K. Taradiy, A. Motornenko, V. Vovchenko, M. I. Gorenstein, and H. Stoecker Phys. Rev. C **100** (2019), 065202; [arXiv:1904.08259 [hep-ph]].
- [55] M. Wakayama, V. G. Bornyakov, D. L. Boyda *et al.*, Phys. Lett. B **793** (2019), 227-233; [arXiv:1802.02014 [hep-lat]].
- [56] J. Takahashi, H. Kouno and M. Yahiro, Phys. Rev. D **91** (2015) no.1, 014501 doi:10.1103/PhysRevD.91.014501 [arXiv:1410.7518 [hep-lat]].
- [57] A. Bazavov, H. T. Ding, P. Hegde, O. Kaczmarek, F. Karsch, E. Laermann, Y. Maezawa, S. Mukherjee, H. Ohno and P. Petreczky, *et al.* Phys. Rev. D **95**, 054504 (2017) [arXiv:1701.04325 [hep-lat]].
- [58] V. Vovchenko, J. Steinheimer, O. Philipsen and H. Stoecker, PoS **CORFU2018**, 199 (2019) [arXiv:1905.01031 [hep-ph]].
- [59] For example, a fit at $T = 265$ MeV starting from a set of initial values $Z_n^{(0)}$ such that $Z_5^{(0)} \div Z_9^{(0)}$ coincide with the respective final values in Table II) and $Z_1^{(0)} \div Z_4^{(0)}$ differ from the respective final values in Table II) by only 1% would not converge to the true minimum but lead to a very large value $\frac{\chi^2}{N_{dof}} = 623$.
- [60] Alternatively, one can use the integration method as described in [18]. The results of these two different procedures coincide for up to 10 ÷ 20 significant digits at least for Z_n at $n < 100$.
- [61] We also determine the model parameters by fitting the summed expressions (19) and (22) to the lattice data for the baryon number and for each model we obtain the parameters identical to those extracted with the truncated series.